

Volumetric and entropic sound sources of Helmholtz resonators attached to a duct with different temperature

Zhenpeng Gan* and Dong Yang†

Southern University of Science and Technology, Shenzhen 518055, Guangdong, China

Helmholtz resonators (HRs) are typical passive control devices employed in practice to damp thermoacoustic instabilities. To protect the HR from the erosion of the hot flow from the combustor, a cooling flow is always injected from the back side of the HR cavity with a temperature much lower than that in the combustor. However, this leads to a dynamic mixing of cold and hot flows in the combustor, which could generate an entropy wave downstream of the HR and influence the HRs' sound absorption performance. In the present paper, an acoustic analogy model for a 1-D combustor duct with different temperature compared to that of the HR attached to it are derived. This model provides physical understanding about the mechanisms of how the presence of the HR and the generation of the entropy wave affect the acoustic fields. It is derived by combining the linearised mass, momentum and energy conservation equations together with a linear Helmholtz resonator model. The model is validated against the results from pre-existing models.

It can be clearly seen from the present acoustic analogy model that the influence of the cooling bias flow of the HR on the 1-D sound field of combustor duct is to provide both a mass-related sound source term and an entropic sound source term. Acoustically, both the mass-related and the entropic source terms are monopole sound sources. A model for the entropy is derived to show that the entropic sound source generated by the mixing process of the cooling bias flow and hot grazing flow is a

*Master student, Department of Mechanics and Aerospace Engineering.

†Associate Professor, Department of Mechanics and Aerospace Engineering. Corresponding author, yangd3@sustech.edu.cn.

negative source compared to the mass-related sound source. If the bias flow temperature is higher than the grazing flow temperature, the mass-related term becomes a positive source. Therefore, the entropy perturbation acts as a positive or negative sound source compared to the mass-related sound source, depending on whether the temperature of bias flow is higher or lower than that of the grazing flow. It is further shown that the overall effect of the mass-related and entropic sound sources is equal to a volumetric source which depends on the mean sound speed and density of the HR instead of those of the combustor.

Nomenclature

C_p	heat capacity at constant pressure, $J/(K \cdot kg)$
C_v	heat capacity at constant volume, $J/(K \cdot kg)$
f_{ref}	resonant frequency, Hz
R_{gas}	the perfect gas constant
S_t	Strouhal number at the neck
I_1	the modified Bessel function of the first
B_1	the modified Bessel function of the second
K_R	Rayleigh conductivity
K_R^t	revised Rayleigh conductivity
$\delta(x)$	Dirac's delta function
r	radius, m
L	neck length, m
A	cross-sectional area, m^2
V	the volume of the HR cavity, m^3
m	mass flux, kg/s
f	momentum flux, $kg \cdot m/s^2$
E	energy flux, $kg \cdot m^2/s^3$
p	pressure, Pa
s	entropy, $J/(K \cdot kg)$
S	Entropy oscillations strength, Pa
t	time, s
x	axial location, m
T	temperature, K
u	velocity, m/s
c	speed of sound, m/s
ω	angular frequency, rad/s

ρ	density, kg/m^3
k	the wavenumber
M	Mach number
γ	heat capacity ratio
Δ	sound absorption coefficient

Abbreviations

<i>SEC</i>	the Dupère and Dowling's stagnation enthalpy continuity model
<i>JC</i>	the Yang and Morgans's Jump condition model
<i>AA</i>	the Acoustic Analogy model
<i>SAA</i>	the Simplified Acoustic Analogy model
<i>OAA</i>	the Original Acoustic Analogy model

Subscripts

$_{HR, h}$	Helmholtz resonator
$_n$	neck of the HR
$_v$	cavity of the HR
$_c$	combustor duct
$_{1, 2, 3}$	section number of the system (here a combustor duct)

Superscripts

$^+$	downstream propagation
$-$	upstream propagation
$'$	time domain oscillation

Overscripts

\sim	Fourier amplitude of oscillation
$\bar{\cdot}$	mean value

I. Introduction

Lean premixed combustion in modern land-based gas turbines and aero-engines is a favorable technology for its performance in considerably decreasing the emission of pollutants, especially NO_x [1]. However, this makes the whole system overwhelmingly vulnerable to thermoacoustic instabilities, which are caused by a positive feedback between the pressure perturbations and the unsteady heat release rate from the combustion [2–5]. This type of feedback can generate large pressure oscillations that may reduce the lifetime of structures or even lead to catastrophic failure [6]. Consequently, the attention of manufacturers has focused on the technologies to predict and damp thermoacoustic instabilities.

In order to suppress these thermoacoustic oscillations, passive damping devices such as Helmholtz resonators (HRs) are widely used to absorb acoustic energy. The Helmholtz resonator and acoustic liner (as shown in Figure 1-6 and 1.3) are both constructed with perforated structures to absorb acoustic energy. One characteristic of this type of hole is the presence of an mean flow (also known as a biased mean flow) in practical situations, such as the flow of cooling gas through perforated liners or Helmholtz resonators in aircraft engines or gas turbines[7–10]. Based on the presence or absence of an mean flow through the hole, the hole models can be divided into linear models (with an average flow) and nonlinear models (without a bias flow). It has been found that the biased flow passing through the hole plays a promoting role in the sound absorption properties of the liner and Helmholtz resonators[7–10]. When a bias flow exists and the Reynolds number is high, the viscous effect is only important near the hole edge, and its main function is to generate vortices[11]. At low frequencies, the sound energy is transferred to the kinetic energy of the vortex shedding: the incident sound wave causes the formation of vortex rings near the hole edge, which are carried away by the mean flow, and the sound energy is transferred to the kinetic energy of the vortices. The energy is dissipated in the subsequent flow due to viscous effects[12]. When there is no bias flow, a nonlinear model is generally utilized to predict the acoustical characteristics of hole pairs, with the absorption characteristics depending on pressure amplitude at the neck exit. The pressure amplitude itself depends on factors such as the incident sound energy, geometric configuration of the combustion chamber, and the location of HR installed in the combustion chamber duct. The nonlinear model proposed by Cummings[13]has been extensively used in both theoretical and experimental studies[9, 14, 15].

It is worth noting that the cooling averaged bias flow through the HR neck or the acoustic lining hole (as shown in Fig. 1.3) in practical applications is often taken from several stages after the compressor, with a temperature range of approximately 500-800 K and a low Mach number (generally not exceeding 0.2) [75]. The temperature of the combustion products in modern gas turbine combustors can reach over 2000 K [76]. This type of hot flow in the combustor passage is known as grazing flow. The influence of grazing flow on the acoustic properties of the HR hole has been extensively studied by numerous researchers [77-82]. The cooling bias flow can protect the Helmholtz resonator and the acoustic lining from erosion by high-temperature gases in the combustor, while also improving its sound absorption performance to some extent. If too little bias flow is added, the neck of the resonator will periodically suck in hot gases. The periodic invasion of hot flow into the cavity of the HR will lead to a periodic change in the fluid density in the neck hole and cavity, causing a frequency shift of the Helmholtz resonator and resulting in its failure. If an excessive amount of cooling bias flow is added, it will change the acoustic impedance of the HR or the acoustic lining,

which will also affect its sound absorption performance and reduce the overall efficiency of the engine. Therefore, the flow velocity of the cooling bias flow should be carefully controlled.

To account for the effect of the temperature difference between the HR and the combustor, Yang and Morgans [16] combined the energy conservation equation with the mass and momentum conservation equations in a 1-D combustor duct, and derived a jump condition model across the HR. This relates the up- and downstream entropy waves and sound waves by a transfer matrix. It shows that the generation of the entropy wave downstream of the HR could significantly change the performance of the resonator. This jump condition model gives the relation between up- and downstream sound and entropy waves, but can not provide the physical mechanism responsible for the changes to the HR's acoustic performance.

Physically, when a Helmholtz resonator is attached to a duct with different temperature, it provides a mass source to the flow inside the duct. As explained on page 8 of Ffowcs Williams [17], “sound production depends crucially on how the mass is created; whether it tends to be done at constant or variable density.” In the present case, the mean density is not constant and an entropy perturbation is generated. In order to correctly identify the sound source (or sink if it’s negative) from the HR, a new model for the acoustic field of the 1-D combustor duct is built in the present paper. This is along the same line as our previous preliminary work in [18]. The present model could account for the influence of the mean density/temperature difference between the HR and the combustor, and the entropy wave downstream of the HR on the sound source, and thus shed light on the mechanisms responsible for the changes to the HR’s acoustic performance.

In section II, based on linearised mass and momentum conservation equations, we derive the governing equation for acoustics with source terms consisting of volumetric and entropic sound sources. Based on linearised mass and energy conservation equations, we developed a model for the entropy perturbation downstream of the resonator. By combining the acoustic governing equation, the model for entropy perturbations and a linear HR model, and solving the problem in the frequency domain, we obtain the analytical solution of the acoustic waves. In section III, the model is applied in test cases with various boundary conditions for given system parameters and validated against the results from pre-existing models. Detailed discussions about the sound sources and the effects of the bias flow temperature (when higher than the grazing flow) are studied in section IV. Finally, the conclusions are given in section V.

II. Theoretical model

A one-dimensional combustion chamber with a Helmholtz resonator installed on the side wall is schematically described in Fig. 1. Where L is the HR neck length, A_c the combustor

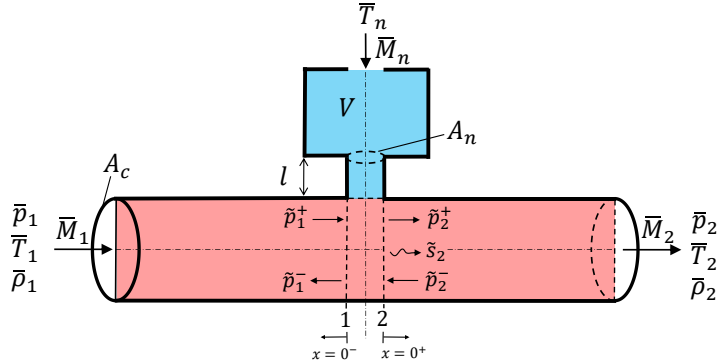


Figure 1: A Helmholtz resonator with different temperatures attached to a combustor duct containing plane acoustic and entropy waves.

duct cross-section area, A_n the HR neck cross-section area, p the pressure, T the temperature, S the entropy wave strength and $\bar{M} = u/c$ the Mach number, with c the speed of sound and u the fluid velocity. Overscripts $\bar{[]}$ and $\tilde{[]}$ denote the mean and oscillation parts of the fluid parameters, respectively. Inside the combustor, subscripts $[]_1$, $[]_2$ and $[]_n$ denote the fluid parameters just before, after the HRs and at the HR neck, respectively. A mean flow with a low Mach number $\bar{M}_{HR} \ll 1$ and temperature \bar{T}_{HR} different from that inside the combustor passes through the HR neck from the back cavity into the combustor.

Assumptions implemented in the present study are:

- (i) the fluids in the system are considered as single-component perfect gases, for which we have the gas law $p = R_{gas}\rho T$,
- (ii) neglecting body forces, any heat addition and thermal diffusion,
- (iii) viscosity is negligible in the main body of the fluid except for near the HR neck region, where its effect is considered by using a HR model,
- (iv) perturbation amplitudes are small so the system is linear,
- (v) the frequency is low so only plane waves are considered in the combustor duct.

The conservation of mass, momentum and energy for this one-dimension combustion duct

gives

$$A_c \left(\frac{\partial \rho}{\partial t} + \frac{\partial(\rho u)}{\partial x} \right) = \delta(x)\dot{m}, \quad (1a)$$

$$A_c \left(\frac{\partial(\rho u)}{\partial t} + \frac{\partial(u^2\rho + p)}{\partial x} \right) = \delta(x)\dot{f}, \quad (1b)$$

$$A_c \left(\frac{\partial[\rho(C_p T + 0.5u^2)]}{\partial t} + \frac{\partial[\rho u(C_p T + 0.5u^2)]}{\partial x} \right) = \delta(x)\dot{E}, \quad (1c)$$

where C_p is the heat capacity at constant pressure which is in general a function of temperature [19], ρ the fluid density, $\delta(x)$ the Dirac delta function, \dot{m} the mass flux source term coming from the HR, \dot{f} the momentum flux source term coming from the HR (assuming that the neck flux is radially inwards with the combustor, so the momentum in the x-direction inside the combustor is constant, i.e. $\dot{f} = 0$) and \dot{E} the energy flux source term coming from the HR.

To obtain the relationship of the mean flow across the resonator junction in combustor, we take the combustion chamber duct between section 1 and section 2 as the control body, as shown in Figure (2-6).

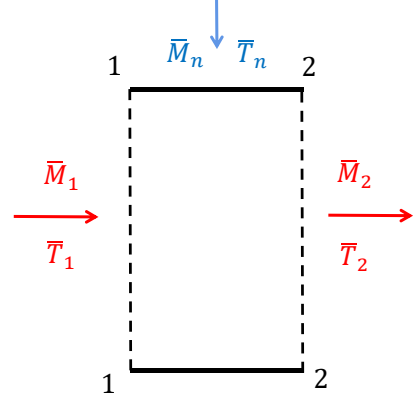


Figure 2: The volume between sections 1-1 and 2-2 served as the control body

Integrating Eqs. 1 from sections 1 to 2 yields the mean flow conservation equations.

$$\bar{\rho}_2 \bar{u}_2 = \bar{\rho}_1 \bar{u}_1 + \bar{\rho}_n \bar{u}_n \frac{A_n}{A_c}, \quad (2a)$$

$$\bar{p}_2 + \bar{\rho}_2 \bar{u}_2^2 = \bar{p}_1 + \bar{\rho}_1 \bar{u}_1^2, \quad (2b)$$

$$\bar{\rho}_2 \bar{u}_2 (C_{p2} \bar{T}_2 + 0.5 \bar{u}_2^2) = \bar{\rho}_1 \bar{u}_1 (C_{p1} \bar{T}_1 + 0.5 \bar{u}_1^2) + \bar{\rho}_n \bar{u}_n (C_{pn} \bar{T}_n + 0.5 \bar{u}_n^2) \frac{A_n}{A_c}. \quad (2c)$$

By giving mean flow parameters upstream the resonator, $\bar{\rho}_1$, \bar{u}_1 and \bar{T}_1 , and combining perfect gas relation, $\bar{\rho}_2$, \bar{u}_2 , \bar{p}_2 and \bar{T}_2 can be obtained. We assume that the temperature in the HR neck is equal to that in its cavity, $\bar{T}_n = \bar{T}_{HR}$, as the cooling flow is usually dominating

the neck flow. Note that the hot gas intrusion can happen when the velocity oscillation at the HR neck is greater than the mean bias flow velocity. Readers are referred to [20–23] for more studies about this. The difference of mean flow parameters before and after the HR is usually very small. This is because the mean mass flux from the HR is generally much smaller than that within the combustor in practical applications (i.e. $\bar{m}_1 \gg \bar{m}_n$, $A_n/A_c \ll 1$). Then the mean flow parameters are assumed to be uniform, such that the mean flow parameters inside combustor can be denoted by subscript $[]_c$ (e.g. $\bar{T}_1 = \bar{T}_2 = \bar{T}_c$).

To obtain the governing equations for the acoustics, Eq. (1a) and Eq. (1b) need to be linearised. Assuming that the perturbation quantities of flow are much smaller than the mean quantities. We can neglect the second or higher order perturbation parameters. By cancelling out the time-average of Eq. (1a) and Eq. (1b), the linearised equations become

$$A_c \left(\frac{\partial \rho'}{\partial t} + \bar{\rho} \frac{\partial u'}{\partial x} + \bar{u} \frac{\partial \rho'}{\partial x} \right) = \delta(x) \dot{m}, \quad (3a)$$

$$\bar{u} \left(\frac{\partial \rho'}{\partial t} + \bar{\rho} \frac{\partial u'}{\partial x} + \bar{u} \frac{\partial \rho'}{\partial x} \right) + \bar{\rho} \frac{\partial u'}{\partial t} + \bar{\rho} \bar{u} \frac{\partial u'}{\partial x} + \frac{\partial p'}{\partial x} = 0. \quad (3b)$$

Due to the dynamic mixing of cold and hot flows, the system will naturally generate entropy waves. Therefore, the density perturbation will include the effect of entropy perturbations. According to the generic thermodynamics relation, the relation between density, pressure and entropy disturbances can be written as

$$\rho' = \frac{p'}{\bar{c}^2} - \frac{\bar{\rho}}{C_p} s', \quad (4)$$

where s' denotes the entropy perturbation. The first and second terms on the right-hand side represent density disturbances due to the pressure and entropy perturbations, respectively.

Take the time derivative of Eq. (3a), subtract the x derivative of Eq. (3b), and substitute Eqs. (4) into it to give

$$\frac{1}{\bar{c}^2} \frac{D^2 p'}{Dt^2} - \frac{\partial^2 p'}{\partial x^2} = \frac{\bar{\rho}}{C_p} \frac{D^2 s'}{Dt^2} + \frac{2\bar{u}}{A_c} \frac{\partial(\dot{m}' \delta(x))}{\partial x} + \frac{1}{A_c} \frac{\partial(\dot{m}' \delta(x))}{\partial t}, \quad (5)$$

where $D/Dt = \partial/\partial t + \bar{u}\partial/\partial x$ denotes the material derivative. This 1-D wave equation takes the form of acoustic analogy: its left-hand side is the equation governing sound propagation and its right-hand side consists of sound source terms caused by entropy (the first term) and mass (the second and third terms) perturbations. The oscillating mass flux through the HR neck causes a monopole sound source inside the combustor. This affects the sound waves in the combustor chamber through the latter two terms on the right-hand side of Eq. (5). Entropy perturbations can also be generated across the HR and this is another monopole

sound source inside the combustor, as shown in the first term on the right-hand side of Eq. (5). The main target of the present paper is to quantitatively study these two kinds of sound sources and their effect on the acoustics of the combustor.

Taking the Fourier transform of Eq. (5), and using the ansatz $[]' = [\tilde{ }]e^{i\omega t}$ where $[\tilde{}]$ denotes the Fourier amplitude gives

$$\left[\left(i\frac{\omega}{\bar{c}} + \bar{M} \frac{\partial}{\partial x} \right)^2 - \frac{\partial^2}{\partial x^2} \right] \tilde{p} = \frac{\bar{\rho}}{C_p} \left(i\omega + \bar{u} \frac{\partial}{\partial x} \right)^2 \tilde{s} + \frac{2\bar{u}}{A_c} \frac{\partial(\tilde{m}\delta(x))}{\partial x} + \frac{i\omega \tilde{m}\delta(x)}{A_c}, \quad (6)$$

where the mean flow velocity is assumed to be in the axial direction, and its effect on the acoustic propagation is usually small under the low-Mach-number condition.

In order to obtain the relation between the up- and downstream pressure disturbances, Eq. (6) needs to be solved. We note that integrating $\tilde{m}(x)\delta(x)$ over x gives the mass flux perturbation from the HR, i.e. \tilde{m}_n , which can be related to the pressure perturbation at the entrance of the HR through an HR model. Entropy perturbation \tilde{s} is unknown and can be obtained by combining \tilde{m}_n with the mass and energy equations. We now introduce an acoustic model for the HR and derive the expression for \tilde{s} .

II.A. A linear Helmholtz resonator model

To relate the mass flux perturbation from the HR neck, \tilde{m}_n , to the pressure perturbation at the HR entrance, we consider a linear HR model. Given an acoustic pressure perturbation at the HR entrance, unsteady vorticity is shed at the edge of the HR neck opening. The mean bias flow sweeps away this shed vorticity, and finally dissipates it into the internal energy of the fluid through viscous effect. The relation between the mass flux perturbation through the HR neck and the pressure difference across it can be expressed in terms of the Rayleigh conductivity [24]

$$K_R = \frac{-\frac{\partial m'_n}{\partial t}}{p'_0 - p'_v}, \quad (7)$$

where p'_0 denotes the oscillating pressure at the entrance of the HR, p'_v the oscillating pressure of the HR cavity, m'_n the mass flow perturbation from the HR into the combustor. K_R is a complex function which can be written as $K_R = 2r_n(\alpha + i\beta)$, and it can be expressed as a function of Strouhal number, according to Howe et al [24].

$$\alpha + i\beta = 1 + \frac{\pi I_1(S_t)e^{-S_t} - 2iB_1(S_t)\sinh(S_t)}{S_t [\pi I_1(S_t)e^{-S_t} + 2iB_1(S_t)\cosh(S_t)]}, \quad (8)$$

where I_1 and B_1 denote the modified Bessel functions of the first and second kinds, $S_t = \omega\sqrt{A_n/\pi}/\bar{u}_v$ the Strouhal number at the neck, and \bar{u}_v the vortex convection velocity which

is approximately equal to the mean velocity at the neck, \bar{u}_n , following Howe [24], Hughes et al. [7] and Eldredge et al. [Eldredge2003absorption].

When a finite neck length is considered, we can use a revised Rayleigh conductivity [Jing1999experimental, Eldredge2003absorption, Scarpato2012modeling, 25] K_R^t given by

$$\frac{1}{K_R^t} = \frac{1}{K_R} + \frac{L}{A_n}, \quad (9)$$

where L denotes the length of HR neck. Equation (9) considers the neck pressure difference being approximately equal to the sum of the contributions from vortex shedding and the acceleration of the fluid inside neck.

Mass conservation for the HR cavity gives

$$\frac{\partial(\rho'_v V)}{\partial t} + m'_n = 0, \quad (10)$$

where V is the volume of the HR cavity, and ρ'_v the density perturbation inside the cavity.

Combining Eqs. (7) and (10), and taking the Fourier transform, we can obtain the relation between the oscillating mass flux \tilde{m}_n at the HR neck and the pressure oscillating \tilde{p}_0 at HR neck entrance. We assume that the pressure oscillation at the HR entrance is equal to that just ahead of it and thus take $\tilde{p}_0 = \tilde{p}_1$ to give

$$\tilde{m}_n = \tilde{p}_1 \mathcal{F}, \quad (11)$$

where $\mathcal{F} = 1/(\bar{c}_v^2/(i\omega V) + i\omega/K_R^t)$, \bar{c}_v denotes the sound speed in the HR cavity.

II.B. A model for the entropy perturbation

In order to obtain the oscillating entropy \tilde{s}_2 , we linearise Eqs. (1a) and (1c) and take the Fourier transform to give

$$\begin{aligned} \tilde{m}_1 + \tilde{m}_n &= \tilde{m}_2, \\ (\bar{m}_2 + \tilde{m}_2) \left[C_{p2}(\bar{T}_2 + \tilde{T}_2) + 0.5(\bar{u}_2^2 + 2\bar{u}_2\tilde{u}_2) \right] &= (\bar{m}_1 + \tilde{m}_1) \left[C_{p1}(\bar{T}_1 + \tilde{T}_1) + 0.5(\bar{u}_1^2 + 2\bar{u}_1\tilde{u}_1) \right] \\ &\quad + (\bar{m}_n + \tilde{m}_n) \left[C_{pn}(\bar{T}_n + \tilde{T}_n) + 0.5(\bar{u}_n^2 + 2\bar{u}_n\tilde{u}_n) \right]. \end{aligned} \quad (12)$$

By combining Eqs. (12) and neglecting the second and higher order perturbations, we

get

$$\begin{aligned}\tilde{T}_2 = & \frac{1}{C_{p2}\bar{m}_2} [\tilde{m}_1(C_{p1}\bar{T}_1 + 0.5\bar{u}_1^2) + \bar{m}_1(\bar{u}_1\tilde{u}_1 + C_{p1}\tilde{T}_1)] \\ & + \frac{1}{C_{p2}\bar{m}_2} [\tilde{m}_n(C_{pn}\bar{T}_n + 0.5\bar{u}_n^2) + \bar{m}_n(\bar{u}_n\tilde{u}_n + C_{pn}\tilde{T}_n)] \\ & - \frac{1}{C_{p2}\bar{m}_2} [(\tilde{m}_1 + \tilde{m}_n)(C_{p2}\bar{T}_2 + 0.5\bar{u}_2^2) + \bar{m}_2\bar{u}_2\tilde{u}_2].\end{aligned}\quad (13)$$

A dimensional analysis shows that $0.5\bar{u}^2$ is $O(\bar{M}^2)$ compared to $C_p\bar{T}$, $\bar{u}\tilde{u}$ is $O(\bar{M})$ compared to $C_p\bar{T}$, $\tilde{m}\bar{T}$ is $O(\bar{M})$ compared to $\bar{m}\tilde{T}$ (for both subscripts $[]_1$ and $[]_n$). As mentioned before, the mean flow is approximately uniform in the combustor, i.e. $C_{p1} = C_{p2} = C_{pc}$ and $\bar{T}_1 = \bar{T}_2 = \bar{T}_c$, so $\tilde{m}_1 C_{p1} \bar{T}_1$ and $-\tilde{m}_1 C_{p2} \bar{T}_2$ cancel out. Equation (13) is then simplified to

$$\tilde{T}_2 = \frac{(C_{pn}\bar{T}_n - C_{pc}\bar{T}_c)\tilde{m}_n + C_{pc}\bar{m}_c\tilde{T}_1}{C_{pc}\bar{m}_c}. \quad (14)$$

The entropy, temperature and pressure perturbations are related by the thermodynamic relation

$$\tilde{T} = \frac{\bar{T}}{C_p} \left(\tilde{s} + \frac{R}{\bar{p}} \tilde{p} \right). \quad (15)$$

We assume that the entropy perturbation at the upstream side of HR, \tilde{s}_1 , is zero. Thus, the temperature perturbation at the upstream side of the HR, \tilde{T}_1 , is given by

$$\tilde{T}_1 = \frac{\bar{T}_c R \tilde{p}_1}{C_{pc} \bar{p}_c}. \quad (16)$$

Similarly, by combining Eqs. (14), (15) and (16), we can obtain the entropy perturbation at the downstream side of the HR,

$$\tilde{s}_2 = \frac{(C_{pn}\bar{T}_n - C_{pc}\bar{T}_c)\tilde{p}_1 \mathcal{F} + A_c \bar{u}_c (\tilde{p}_1 - \tilde{p}_2)}{T_c \bar{m}_c}. \quad (17)$$

This expression shows that the entropy oscillation at the downstream side of the HR depends on the mean flow parameters of the HR and the combustor, and the pressure perturbation amplitudes on each side of the HR.

II.C. The solution of the system

We now combine the models for the HR and the entropy perturbation with Eq. (6) to get the solution of the system. Equation (6) degenerates to a homogeneous equation in the regions up- and downstream of the HR (in $x < 0$ and $x > 0$ respectively), where the general

solutions can be written as

$$\tilde{p}_1 = \tilde{p}_1^+ e^{ik^+ x} + \tilde{p}_1^- e^{ik^- x}, \quad (18a)$$

$$\tilde{p}_2 = \tilde{p}_2^+ e^{ik^+ x} + \tilde{p}_2^- e^{ik^- x}, \quad (18b)$$

where k^+ and k^- denote the wavenumber

$$\begin{aligned} k^+ &= -\frac{\omega}{\bar{c} + \bar{u}}, \\ k^- &= \frac{\omega}{\bar{c} - \bar{u}}. \end{aligned} \quad (19)$$

Integrating Eqs. (6) with respect to x from 0^- to 0^+ once and twice gives

$$(1 - \bar{M}_c^2) \left. \frac{\partial \tilde{p}}{\partial x} \right|_1^2 = i\omega \left[\frac{2\bar{M}_c}{\bar{c}_c} (\tilde{p}_1 - \tilde{p}_2) + \frac{\bar{\rho}_c}{Cp_c} \bar{u}_c \tilde{s}_2 + \frac{\tilde{m}_n}{A_c} \right], \quad (20a)$$

$$(1 - \bar{M}_c^2) \tilde{p}|_1^2 = \frac{\bar{\rho}_c}{Cp_c} \bar{u}_c^2 \tilde{s}_2 + 2\bar{u}_c \frac{\tilde{m}_n}{A_c}. \quad (20b)$$

The first term in the square bracket on the right-hand side of Eq. (20a) comes from the mean Mach-number term on left-hand side of Eq. (6), and is negligible due to the low-Mach-number assumption. The later two terms on the right-hand side in the square bracket of Eq. (20a) are the entropy-related sound source and mass-related sound source, respectively.

We now have 6 equations, Eqs. (11), (17), (18a), (18b), (20a) and (20b) and 8 unknown perturbation parameters, \tilde{p}_1 , \tilde{p}_2 , \tilde{p}_1^+ , \tilde{p}_1^- , \tilde{p}_2^+ , \tilde{p}_2^- , \tilde{m}_n and \tilde{s}_2 in this set of equations. Therefore, 2 boundary conditions need to be added. Two more conditions of perturbation parameters of \tilde{p}_1^+ , \tilde{p}_1^- , \tilde{p}_2^+ , \tilde{p}_2^- are usually given as the boundary conditions. In the next section, we are going to discuss the solution of the equations in 3 cases considering different boundary conditions.

III. Case study and comparisons with previous models

We now apply the theoretical model to several test cases to study the effect of the temperature difference between the HR and the combustor on the acoustics inside the combustor. Comparisons with previous models are performed to validate the present model. The geometry and mean flow parameters involved are summarized in Table 1. Different acoustic boundary conditions are considered in the following cases.

Table 1: Geometry and mean flow parameters of the HR and combustor

HR	Neck length (L/m)	5×10^{-3}
	Neck sectional area (A_n/m^2)	1×10^{-4}
	Mean Cavity temperature (\bar{T}_n/K)	500,750,1000
	Cavity volume (V/m^3)	2.5×10^{-4}
	Mean neck Mach number(\bar{M}_n)	1×10^{-2}
Combustor	Duct area (A_n/m^2)	$\pi \times 10^{-2}$
	Upstream mean pressure (\bar{p}_1/Pa)	2×10^6
	Upstream mean temperature (\bar{T}_1/K)	1000
	Mean upstream Mach number (\bar{M}_1)	3×10^{-2}

III.A. Case I

We firstly assume that the ducts both up- and downstream the HR are infinitely long, the downstream propagating acoustic wave before the HR is given and the upstream propagating wave downstream the HR is zero, i.e. $\tilde{p}_1^+ = 100Pa$ and $\tilde{p}_2^- = 0$.

By combining Eqs. (11), (17), (18a), (18b), (20a) and (20b), we get

$$\tilde{p}_1^- = \frac{\left[\bar{M}^2(1 + \gamma) + \frac{\bar{M}}{1+\bar{M}} + \frac{C_{pn}\bar{T}_n}{C_{pc}\bar{T}_c}(2\bar{M}^2 + \frac{1+2\bar{M}}{1+\bar{M}}) \right] \frac{\mathcal{F}}{A_c}}{\frac{2[(1-\gamma)\bar{M}^2+1]}{\bar{c}(1-\bar{M}^2)} - \left[\bar{M}^2(1 + \gamma) + \frac{\bar{M}}{1+\bar{M}} + \frac{C_{pn}\bar{T}_n}{C_{pc}\bar{T}_c}(2\bar{M}^2 + \frac{1+2\bar{M}}{1+\bar{M}}) \right] \frac{\mathcal{F}}{A_c}} \tilde{p}_1^+, \quad (21a)$$

$$\tilde{p}_2^+ = \frac{\frac{2[(1-\gamma)\bar{M}^2+1]}{\bar{c}(1-\bar{M}^2)} - \frac{2\bar{M}}{1-\bar{M}^2} \left(\frac{C_{pn}\bar{T}_n}{C_{pc}\bar{T}_c} + 1 \right) \frac{\mathcal{F}}{A_c}}{\frac{2[(1-\gamma)\bar{M}^2+1]}{\bar{c}(1-\bar{M}^2)} - \left[\bar{M}^2(1 + \gamma) + \frac{\bar{M}}{1+\bar{M}} + \frac{C_{pn}\bar{T}_n}{C_{pc}\bar{T}_c}(2\bar{M}^2 + \frac{1+2\bar{M}}{1+\bar{M}}) \right] \frac{\mathcal{F}}{A_c}} \tilde{p}_1^+, \quad (21b)$$

$$\tilde{s}_2 = \frac{(C_{pn}\bar{T}_n - C_{pc}\bar{T}_c) + \bar{u}_c^2 \left(\frac{C_{pn}\bar{T}_n}{C_{pc}\bar{T}_c} + 1 \right)}{\bar{T}_c \bar{m}_c} \mathcal{F}(\tilde{p}_1^+ + \tilde{p}_1^-). \quad (21c)$$

This is the analytical solution of our Acoustic Analogy model (denoted as AA model here after). Equation (21c) shows that the entropy perturbation depends on the mean temperature, the heat capacity at constant pressure and the pressure oscillation at the HR inlet. A dimensional analysis shows that the second term in the numerator of Eq. (21c) is $O(M^2)$ compared the first term, hence can be neglected. Physically, it indicates that the first term, which represents the dynamic mixing of cold and hot flows, is the dominant mechanism responsible for the generation of entropy perturbations. If terms of orders higher than $O(M)$

are neglected in Eqs. (21), we can get

$$\tilde{p}_1^- = \frac{\frac{1}{1+\bar{M}} \left[\frac{C_{pn}\bar{T}_n}{C_{pc}\bar{T}_c} (1+2\bar{M}) + \bar{M} \right] \frac{\mathcal{F}}{A_c}}{\frac{2}{\bar{c}} - \frac{1}{(1+\bar{M})} \left[(1+2\bar{M}) \frac{C_{pn}\bar{T}_n}{C_{pc}\bar{T}_c} + \bar{M} \right] \frac{\mathcal{F}}{A_c}} \tilde{p}_1^+, \quad (22a)$$

$$\tilde{p}_2^+ = \frac{\frac{2}{\bar{c}} - 2\bar{M} \left(\frac{C_{pn}\bar{T}_n}{C_{pc}\bar{T}_c} + 1 \right) \frac{\mathcal{F}}{A_c}}{\frac{2}{\bar{c}} - \frac{1}{(1+\bar{M})} \left[(1+2\bar{M}) \frac{C_{pn}\bar{T}_n}{C_{pc}\bar{T}_c} + \bar{M} \right] \frac{\mathcal{F}}{A_c}} \tilde{p}_1^+, \quad (22b)$$

$$\tilde{s}_2 = \frac{C_{pn}\bar{T}_n - C_{pc}\bar{T}_c}{\bar{T}_c \bar{m}_2} \mathcal{F}(\tilde{p}_1^+ + \tilde{p}_1^-), \quad (22c)$$

Equations (22) are called the Simplified Acoustic Analogy model (denoted as SAA model here after). We want to note that the assumption that the terms of order $O(\bar{M}^2)$ and higher can be neglected is fairly unrestricted for gas turbine combustors where \bar{M} is normally smaller than 0.3. The effect of the mean grazing flow Mach number is studied further in Appendix VI.A

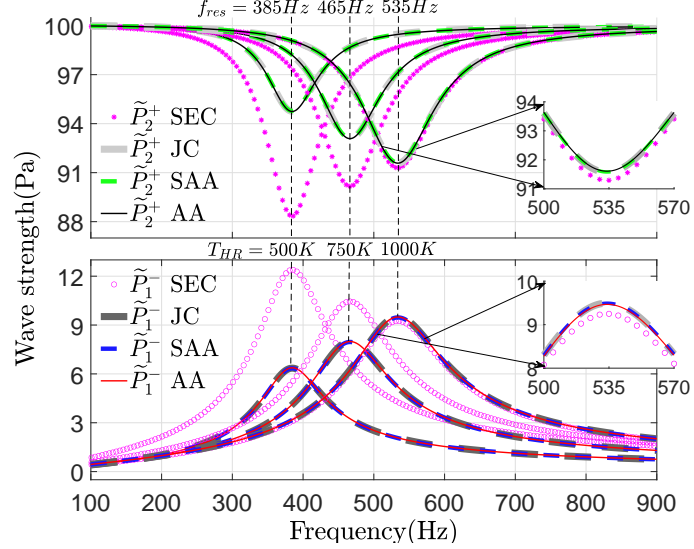
In the following, results from the present AA and SAA models are compared against those from the Yang and Morgans' Jump condition model (JC) [16] and Dupère and Dowling's model assuming continuous stagnation enthalpy oscillation (SEC) [14]. The readers are referred to these two papers for detailed derivations of these two models.

Figure 3 shows the acoustic and entropy wave strengths and the HR's sound absorption coefficient from the present and pre-existing models. We have kept the combustor temperature at 1000K and set the bias flow temperature to increase from 500K, 750K up to 1000K which means that the resonant frequencies of the HR is approximately 385Hz, 465Hz, 535Hz, respectively. It can be clearly seen how the HR with various temperatures affect the overall acoustic field when giving an incident acoustic perturbation.

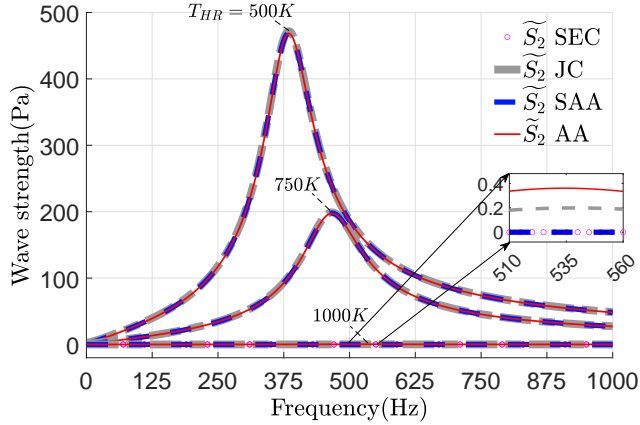
As shown in Fig. 3a (bottom), for all temperatures, the strength of the reflected wave before the HR, \tilde{p}_1^- , firstly increases with frequency at low frequencies, reaches its maximum at the resonant frequency and decreases with frequency above the resonant frequency. The strength of downstream-propagating wave strength after the HR, \tilde{p}_2^+ , decreases at low frequencies, reaches its minimum, and returns to 100Pa above the resonant frequency, as shown in Fig. 3a (top). These trends are captured by all models. When \bar{T}_{HR} increases, both the present AA and SAA models predict increased maximums in \tilde{p}_1^- and decreased minimums in \tilde{p}_2^+ at resonant frequencies. This agrees with the Jump condition model in [16]. However, the stagnation continuity model (SEC) does not consider temperature difference and gives the opposite trends.

Regarding the HR temperature of 500K, the amplitude of \tilde{p}_1^- from the SEC model is almost the double of those from the JC, AA and SAA models. When $\bar{T}_{HR} = 1000K$, there is no temperature difference between the combustor and the HR, and all models give similar

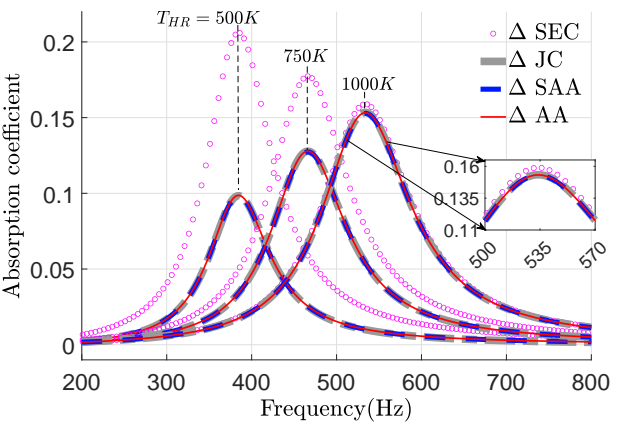
acoustic wave strengths.



(a) Case I Acoustic wave strengths



(b) Case I Entropy wave strength



(c) Case I Absorption coefficient

Figure 3: Case I $\tilde{p}_1^+ = 100\text{Pa}$ and $\tilde{p}_2^- = 0$. The acoustic and entropy wave strengths and absorption coefficient for the HR with a cavity temperature of 500, 750, 1000K, while the combustor temperature is kept at 1000K.

We define the entropy wave strength as $\tilde{S}(x) = \tilde{s}(x)(\gamma-1)\bar{\rho}\bar{T}$ in which $\tilde{s} = C_v\tilde{p}/\bar{p} - C_p\tilde{\rho}/\bar{\rho}$ denotes the oscillating entropy. Figure 3b shows that in general all the curves of predicted entropy wave strength reach the maximum value at their resonant frequency in the presence of temperature difference (i.e. $\bar{T}_{HR} = 500\text{K}$ and $\bar{T}_{HR} = 750\text{K}$), and decrease away from this frequency, with exception of the SEC model which stays at about zero. This means that the SEC model predicts zero entropy generation, while the present AA and SAA model predict significant entropy perturbations near the resonant frequency. The results from the AA and SAA models agree well with those from the previous JC model. Moreover, the peak of entropy this oscillation increases significantly with the increase of temperature difference

$(\Delta \bar{T} = \bar{T}_{HR} - \bar{T}_c)$. In the absence of temperature difference (i.e. $\bar{T}_{HR} = 1000K$) there is little generated entropy wave.

As shown in Figure 3c, in the absence of temperature difference ($\bar{T}_{HR} = 1000K = \bar{T}_c$) the HR's sound absorption coefficient reaches its peak at resonant frequency and decreases gradually away from resonance. In this case, all the four models give the same prediction about the HR's sound absorption coefficient [26]:

$$\Delta = 1 - \frac{|\tilde{p}_1^-|^2(1 - \bar{M}_1)^2 + |\tilde{p}_2^+|^2(1 + \bar{M}_2)^2}{|\tilde{p}_1^+|^2(1 + \bar{M}_1)^2 + |\tilde{p}_2^-|^2(1 - \bar{M}_2)^2}. \quad (23)$$

which denotes the percent of the absorbed sound energy over the incident sound energy. With the declining of the HR temperature the sound absorption coefficient from the four models still show a similar trend for each temperature, but those from AA, SAA and JC models capture the effect of temperature difference and see a significant decrease of the peak value, while the SEC model does not consider the temperature difference and gives the opposite trend.

The present AA, SAA and the JC models show good agreements in these results. Their slight difference is of the order $O(\bar{M}^2)$, and is discussed in Appendix VI. It can be seen that the SAA model, which is simplified from the AA model by further neglecting the terms of orders higher than $O(\bar{M})$, is accurate enough compared to the AA model under the low-Mach-number condition considered in the present study. Hence, the following cases only compare the results from the SAA, JC and SEC models.

III.B. Case II

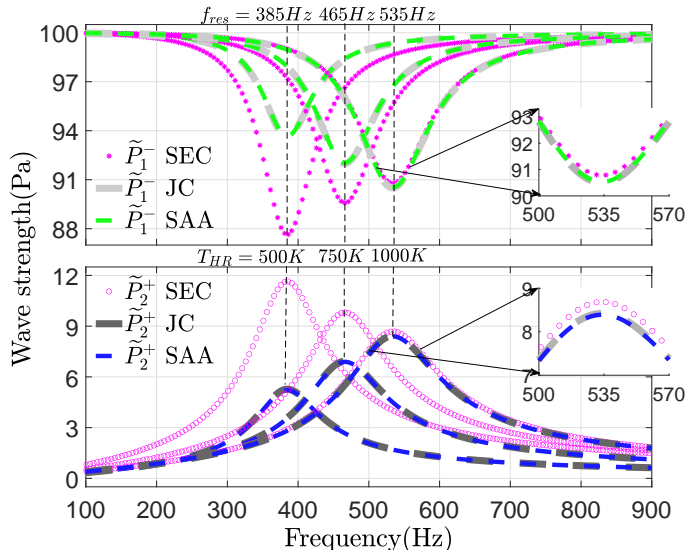
In this case, the combustor duct is still assumed to be semi-infinitely long both up- and downstream of the HR but we now assume $\tilde{p}_2^- = 100Pa$ and $\tilde{p}_1^+ = 0Pa$. By following the same procedure as case I, we can solve \tilde{p}_1^- , \tilde{p}_2^+ and \tilde{s}_2 and then by neglecting terms of orders higher than $O(\bar{M})$, we can write \tilde{p}_1^- , \tilde{p}_2^+ and \tilde{s}_2 as

$$\tilde{p}_1^- = \frac{\frac{2}{\bar{c}}}{\frac{2}{\bar{c}} - \left[\frac{1+2\bar{M}}{1+\bar{M}} \frac{C_{pn}\bar{T}_n}{C_{pc}\bar{T}_c} + \frac{\bar{M}}{1+\bar{M}} \right] \frac{\mathcal{F}}{A_c}} \tilde{p}_2^-, \quad (24a)$$

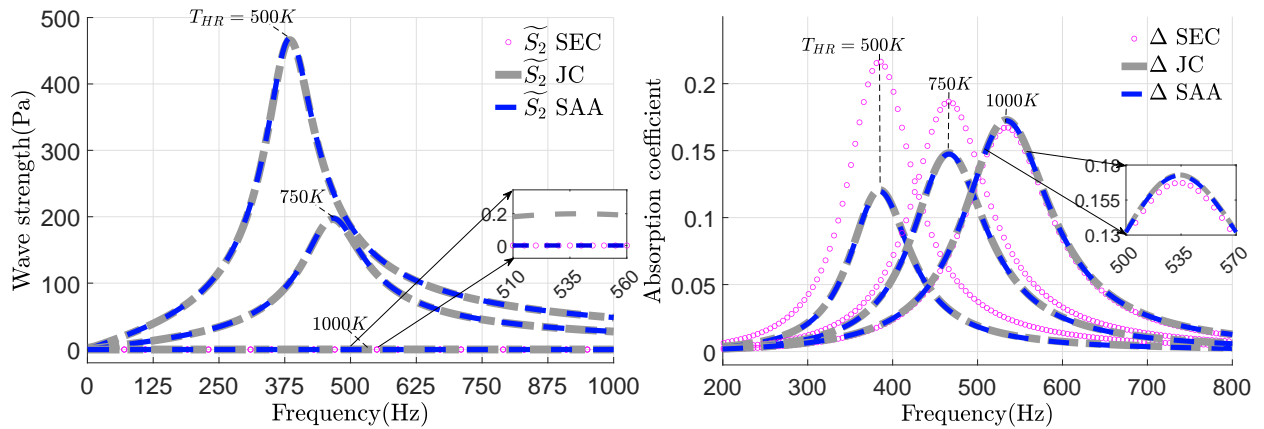
$$\tilde{p}_2^+ = \frac{\left[\frac{1-2\bar{M}}{1-\bar{M}} \frac{C_{pn}\bar{T}_n}{C_{pc}\bar{T}_c} - \frac{\bar{M}}{1-\bar{M}} \right] \frac{\mathcal{F}}{A_c}}{\frac{2}{\bar{c}} - \left[\frac{1+2\bar{M}}{1+\bar{M}} \frac{C_{pn}\bar{T}_n}{C_{pc}\bar{T}_c} + \frac{\bar{M}}{1+\bar{M}} \right] \frac{\mathcal{F}}{A_c}} \tilde{p}_2^-, \quad (24b)$$

$$\tilde{s}_2 = \frac{C_{pn}\bar{T}_n - C_{pc}\bar{T}_c}{\bar{T}_c \bar{m}_2} \mathcal{F} \tilde{p}_1^-. \quad (24c)$$

In this case, it can be seen in Fig. 4 that the results follow almost the same trend as case I, because they both give an incident acoustic wave with the same amplitudes in an



(a) Case II Acoustic wave strengths



(b) Case II Entropy wave strength

(c) Case II Absorption coefficient

Figure 4: Case II $\tilde{p}_1^+ = 0$ and $\tilde{p}_2^- = 100 \text{ Pa}$. The acoustic and entropy wave strengths and absorption coefficient for the HR with a cavity temperature \bar{T}_{HR} of 500K, 750K, 1000K, while the combustor temperature \bar{T}_c is 1000K.

infinitely long duct. The slight difference is because, the given incident acoustic wave in case I is propagating towards the HR in the same direction as the grazing flow but is in the opposite direction in case II. This difference will increase with the Mach number of the grazing flow.

III.C. Case III

We now assume that the combustor upstream the HR has a finite length, and \tilde{p}_1^+ just ahead of the HR is given and $\tilde{p}_1^- = \tilde{p}_1^+ e^{i\theta}$. By following a similar procedure as case I and case II, we can solve \tilde{p}_2^- , \tilde{p}_2^+ and \tilde{s}_2 . By neglecting terms of orders higher than $O(\bar{M})$, the results are

$$\begin{aligned}\tilde{p}_2^+ &= \tilde{p}_1^+ + \frac{\bar{c}}{2(1-\bar{M})} \left[(1-2\bar{M}) \frac{C_{pn}\bar{T}_n}{C_{pc}\bar{T}_c} - \bar{M} \right] \frac{\mathcal{F}}{A_c} (\tilde{p}_1^+ + \tilde{p}_1^-), \\ \tilde{p}_2^- &= \tilde{p}_1^- - \frac{\bar{c}}{2(1+\bar{M})} \left[(1+2\bar{M}) \frac{C_{pn}\bar{T}_n}{C_{pc}\bar{T}_c} + \bar{M} \right] \frac{\mathcal{F}}{A_c} (\tilde{p}_1^+ + \tilde{p}_1^-), \\ \tilde{s}_2 &= \frac{C_{pn}\bar{T}_n - C_{pc}\bar{T}_c}{\bar{T}_c \bar{m}_2} \mathcal{F} (\tilde{p}_1^+ + \tilde{p}_1^-).\end{aligned}\quad (25)$$

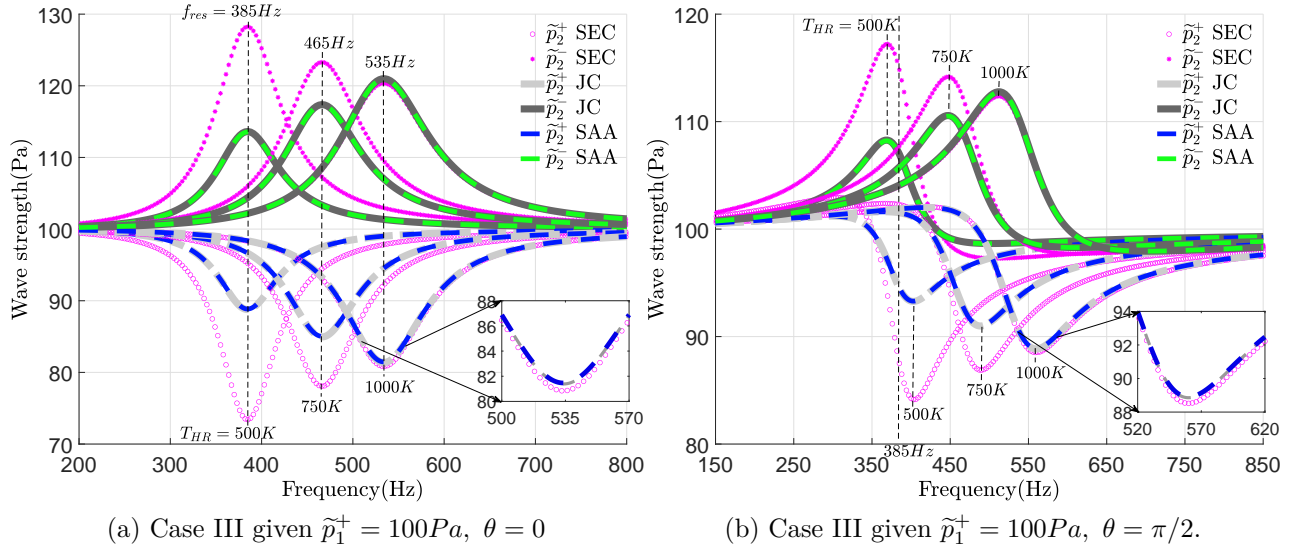


Figure 5: Case III given $\tilde{p}_1^+ = 100Pa$, $\tilde{p}_1^- = \tilde{p}_1^+ e^{i\theta}$. The acoustic wave strengths for the HR with a cavity temperature \bar{T}_{HR} of 500K, 750K, 1000K, while the combustor temperature keeps \bar{T}_c at 1000K.

Figures 5a and 5b show the acoustic wave strengths from the present and pre-existing models when θ is equal to 0 and $\pi/2$, respectively. This distinctly displays the influence of the HR installation position on the overall sound field. Other parameters are the same as case I.

Setting $\theta = 0$ means that the HR is installed at a pressure anti-node. The results in

Fig. 5a show that introducing an HR gives a maximum value of \tilde{p}_2^- and a minimum value of \tilde{p}_2^+ near the resonant frequency of the HR. This resonant frequency increases with the HR temperature. It can be seen that the predicted acoustic wave strengths from the present SAA model matches those from the JC model for all temperatures. The amplitude of \tilde{p}_2^- predicted by the SEC model greatly exceeds those from the other two models, and \tilde{p}_2^+ predicted by the SEC model is significantly lower than those from the other two models. These differences diminish when the HR temperature is increased to 1000K. For the present SAA and JC models, increasing the HR temperature would increase the difference between \tilde{p}_2^- and \tilde{p}_2^+ downstream of the HR, while the SEC model gives the opposite results.

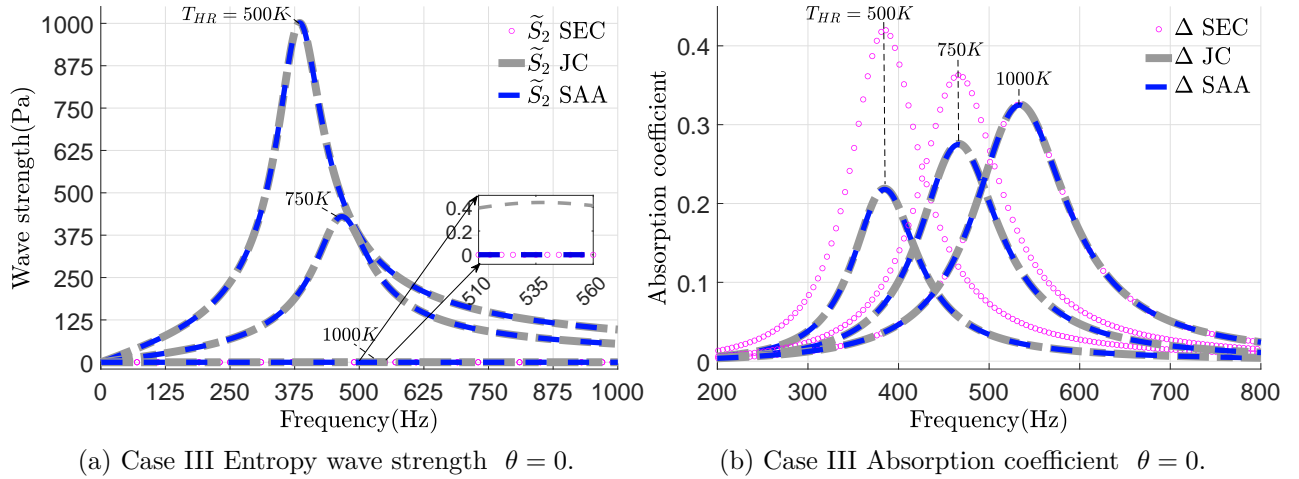


Figure 6: Case III given $\tilde{p}_1^+ = 100Pa$, $\theta = 0$. The entropy wave strength (a) and acoustic absorption coefficient (b) for the HR with a cavity temperature T_{HR} of 500K, 750K, 1000K, while the combustor temperature \bar{T}_c keeps at 1000K.

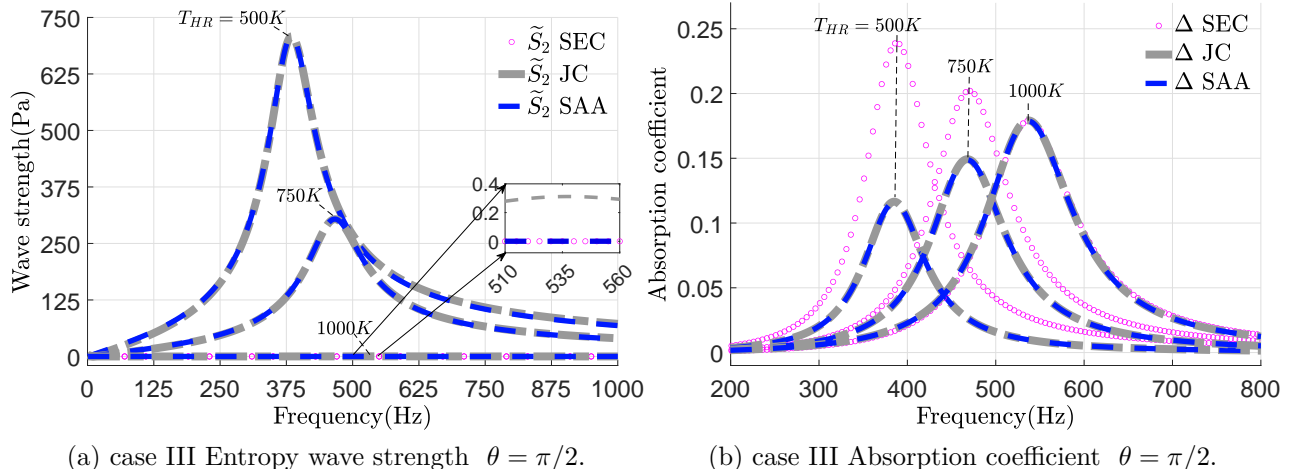


Figure 7: Case III given $\tilde{p}_1^+ = 100Pa$, $\theta = \pi/2$. The entropy wave strength (a) and acoustic absorption coefficient (b) for the HR with a cavity temperature T_{HR} of 500K, 750K, 1000K, while the combustor temperature \bar{T}_c keeps at 1000K.

Regrading the $\theta = \pi/2$ case, as shown in Fig. 5b, each acoustic wave strength sees a similar trend as that in the $\theta = 0$ case, except that a phase difference between the peaks of the up- and downstream-propagating acoustic waves at the downstream side of the HR is seen; compared to the $\theta = 0$ case, the $\theta = \pi/2$ case moves the peak of \tilde{p}_2^- to a slightly lower frequency and the minimum of \tilde{p}_2^+ to a slightly higher frequency.

The entropy wave strength and the acoustic absorption coefficient of the HR when \bar{T}_{HR} varies from 500K to 1000K and $\bar{T}_c = 1000K$ are shown in Figs. (6) and (7), respectively. The present SAA model's predictions agree well with the JC model being consistent with those found in cases I and II.

IV. Discussions about the sound sources

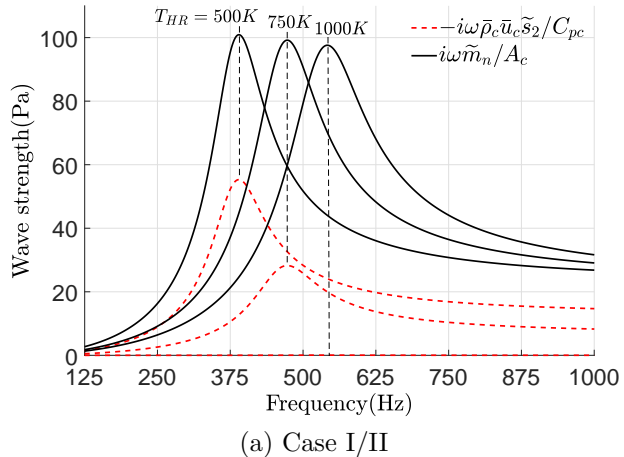
IV.A. What are the true sound sources?

As shown in section III, the temperature difference between the HR and the combustor has a strong impact on the relation between the acoustic and entropy waves before and after the HR. The unsteady injection of bias flow with a different temperature produces an entropic and a mass-related sound sources simultaneously to affect the acoustic field inside the combustor.

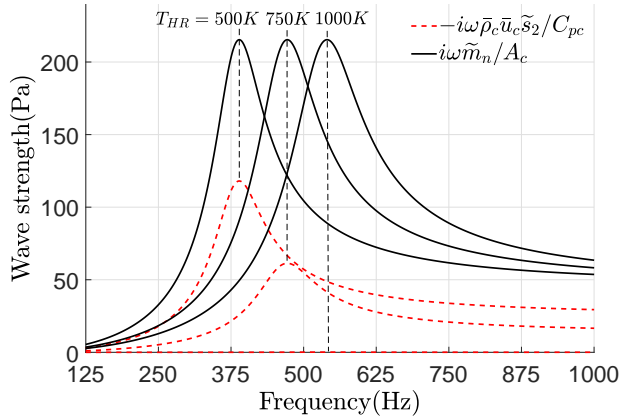
The amplitude of second and third sound source terms on the right-hind side of Eq. (20a) for different cases are shown in Fig. 8. It can be seen that at the resonant frequency when $\bar{T}_{HR} = 500K$, the two source terms reach their peaks, decrease when the frequency is further increased. With the increase of the HR temperature, the peak value of the entropy-related source term decreases significantly (to zero when $\bar{T}_{HR} = 1000K$).

By comparing Figs. 8a, 8b and 8c, it is clear that the ratio between the entropy-related source term and the mass-related source term is independent of the location of the HR and the given incident sound pressure but depends on the temperature difference between the HR and the combustor. The entropy-related source term is negative compared to the mass-related source term when $\bar{T}_{HR} < \bar{T}_c$.

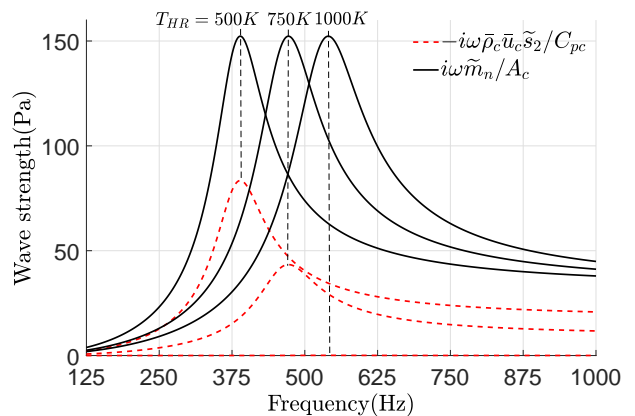
There is a significant difference between the SEC model and the present model in the presence of temperature difference. This is because the entropy-related source term acts as a negative monopole sound source which counteracts part of the acoustic effect induced by merely the unsteady mass injection from the HR. Consequently, the acoustic effect associated with the entropy-related source will counteract that associated with the mass-related source. This explains the difference between the SEC and the present models, as shown in Figs. 3a, 4a and 5. For example, in case III, this is what makes the peak of the upstream-propagating acoustic wave strength, \tilde{p}_2^- , in the present model smaller than that of the SEC model, and the downstream-propagating wave, \tilde{p}_2^+ , in the present model greater than that of the SEC



(a) Case I/II



(b) Case III given $\tilde{p}_1^+ = 100Pa, \theta = 0$



(c) Case III given $\tilde{p}_1^+ = 100Pa, \theta = \pi/2$

Figure 8: The entropy- and mass-related source terms in Eq. (20) for various cases with the HR temperature \bar{T}_{HR} ranging from 500K to 1000K. (a) shows the strength of source terms in case I or case II, because they followed the same picture.

model, as can be seen in Fig. 5. As a result, the HR's sound absorption coefficient predicted by the present model is lower than that from the SEC model in the presence of temperature difference.

Obviously, the predictions about the acoustic, entropy waves and the sound absorption coefficient from the stagnation enthalpy continuity (SEC) model is inaccurate because it does not take the temperature difference into account. And hence, the effect on the acoustic wave induced by the entropic source is missing. This means that the overall acoustic source not only depends on the effect of the unsteady mass injection from the HR but also on the effect of temperature/density discontinuity. In order to more clearly identify the sound sources of the HR, we now conduct the following derivations to show how the mass- and entropy-related source terms contribute separately as monopole sound sources to the 1-D duct acoustics in the combustor.

The linearised Euler equations with no mass sources are

$$\frac{\partial \rho'}{\partial t} + \frac{\partial(\bar{\rho}u' + \bar{u}\rho')}{\partial x} = 0, \quad (26a)$$

$$\frac{\partial(\bar{\rho}u' + \bar{u}\rho')}{\partial t} + \frac{(2\bar{\rho}\bar{u}u' + \bar{u}^2\rho')}{\partial x} + \frac{\partial p'}{\partial x} = 0. \quad (26b)$$

By substituting Eq. (26a) into Eq. (26b) and assuming that the Mach number is low we get

$$\left. \frac{\partial \tilde{p}}{\partial x} \right|_1 \cdot \frac{1}{i\omega \bar{\rho}_c} = \tilde{u}|_1^2 \quad (27)$$

It is obvious that the left-hand-side term represents the net outflux volume between interfaces 1 and 2. This is the volumetric sound source between 1 and 2. The difference of the pressure gradient between 1 and 2 on left-hand-side can be substituted by Eq. (20a). Then, by neglecting terms of orders higher than $O(\bar{M})$, incorporating Eq. (22c) and assuming $\bar{p}_n \approx \bar{p}_c$ and $\bar{C}_{pn} \approx \bar{C}_{pc}$ as well as defining the dimensionless impedance of the HR as $Z_{HR} = \tilde{p}_1 / (\tilde{u}_n \bar{\rho}_n \bar{c}_n)$, we get

$$\begin{aligned} \tilde{u}|_1^2 &= \frac{\bar{u}_c}{C_{pc}} \tilde{s}_2 + \frac{\tilde{m}_n}{\bar{\rho}_c A_c} \\ &= \left(\frac{C_{pn} \bar{T}_n}{C_{pc} \bar{T}_c} - 1 \right) \cdot \frac{\tilde{m}_n}{\bar{\rho}_c A_c} + \frac{\tilde{m}_n}{\bar{\rho}_c A_c} \\ &= \frac{C_{pn} \bar{T}_n}{C_{pc} \bar{T}_c} \cdot \frac{\tilde{m}_n}{\bar{\rho}_c A_c} \\ &\approx \frac{\bar{\rho}_c}{\bar{\rho}_n} \cdot \frac{\tilde{m}_n}{\bar{\rho}_c A_c} = \frac{\tilde{m}_n}{\bar{\rho}_n A_c} = \frac{\tilde{p}_1}{Z_{HR} \bar{\rho}_n \bar{c}_n} \cdot \frac{A_n}{A_c}. \end{aligned} \quad (28)$$

It is not surprising to see from the last step of Eq. (28) that the overall sound source

to the acoustics in the combustor duct is equivalent to the volumetric sound source coming from the HR. However, it is not straightforward to understand that in the presence of a temperature difference between the HR and the combustor, the generation of an entropy wave is a necessary condition for this to be guaranteed. Furthermore, it is worth noting that this volumetric sound source is calculated by using the mean speed of sound and density of where it comes from (the HR) instead of where it goes (the combustor).

The pressure perturbation is usually assumed to be approximately continuous across the HR, we now briefly show that this is true in the present cases. By combining Eq. (24a) and Eq. (20) with the boundary condition we can get the difference between the oscillating pressure upstream and downstream of the HR

$$\tilde{p}_1 - \tilde{p}_2 = \left(\frac{C_{pn}\bar{T}_n}{C_{pc}\bar{T}_c} + 1 \right) \frac{\bar{u}_c \mathcal{F}}{A_c} \tilde{p}_1. \quad (29)$$

Dimensional analysis reveals that term $\bar{u}_c \mathcal{F}/A_c$ is of order of $O(\bar{M}^3)$ near the resonant frequency and is of the order $O(\bar{M})$ away from the resonant frequency. Hence, $\tilde{p}_1 - \tilde{p}_2$ is at least $O(\bar{M})$ smaller than \tilde{p}_1 and the pressure perturbation can be considered to be continuous across the HR.

With this in mind, it can be seen that the first term in the square bracket of Eq. (20a) is $O(\bar{M}^2)$ smaller than the other two terms in the same bracket, so it can be neglected. Furthermore, if all the terms of orders higher than $O(\bar{M})$ are neglected, Eqs. (11), (17) and (20) can be combined to give

$$\left. \frac{\partial \tilde{p}}{\partial x} \right|_1^2 = i\omega \left(\frac{\bar{\rho}_c}{C p_c} \bar{u}_c \tilde{s}_2 + \frac{\tilde{m}_n}{A_c} \right) = i\omega \frac{C_{pn}\bar{T}_n}{C_{pc}\bar{T}_c} \frac{\tilde{m}_n}{A_c}, \quad (30a)$$

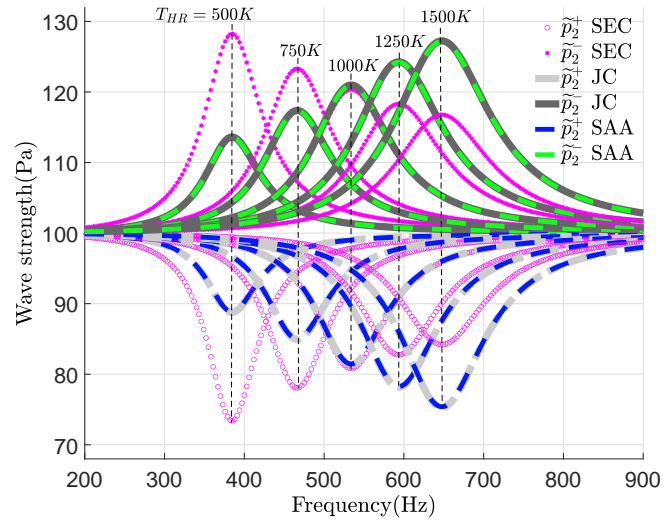
$$\tilde{p}|_1^2 = \bar{u}_c \left(\frac{\bar{\rho}_c}{C p_c} \bar{u}_c \tilde{s}_2 + 2 \frac{\tilde{m}_n}{A_c} \right) = \bar{u}_c \left(\frac{C_{pn}\bar{T}_n}{C_{pc}\bar{T}_c} + 1 \right) \frac{\tilde{m}_n}{A_c}. \quad (30b)$$

This is the same as our Simplified Acoustic Analogy model (SAA), solving this simplified model gives the same expressions as Eqs. (22), (24) and (25). From Eq. (30a), we can also obtain the same conclusions as that from Eq. (28).

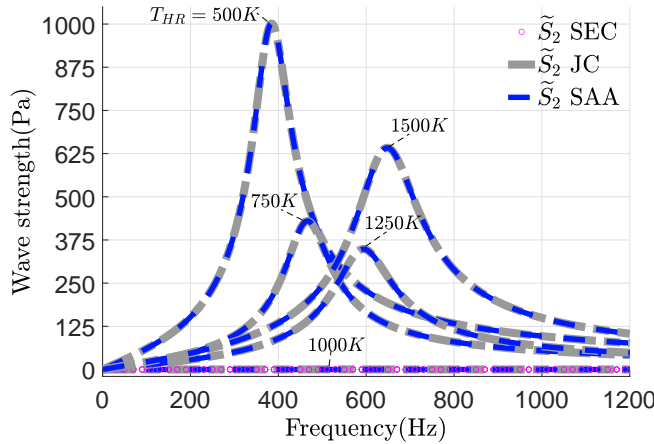
IV.B. The effect of higher-temperature bias flow

A cooled HR sees a reduced sound absorption coefficient, because the entropic sound source counteracts the mass-related source, as explained before. It would then be natural to see an increased sound absorption performance if the bias flow has a higher temperature than the grazing flow.

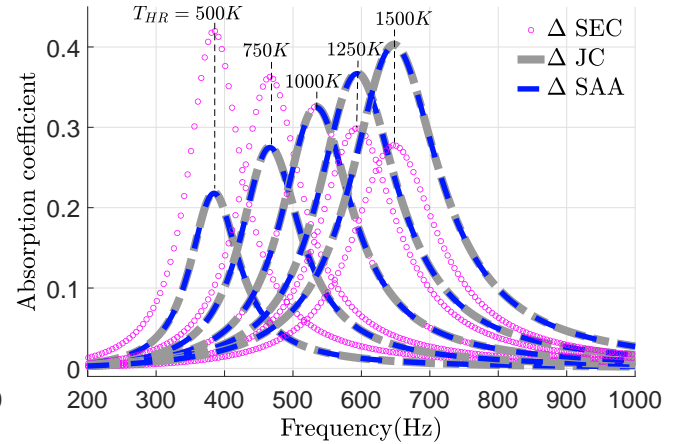
Figure 9 compares the results of from the SEC, JC and SAA models when increasing the



(a) Acoustic wave strengths



(b) Entropy wave strength



(c) Sound absorption coefficient

Figure 9: Case III given $\tilde{p}_1^+ = \tilde{p}_1^- = 100\text{Pa}$, $\theta = 0$. The acoustic, entropy wave strengths and sound absorption coefficient for increasing the temperature of the bias flow from 500K up to 1500K, while the grazing flow temperature remains constant at 1000 K

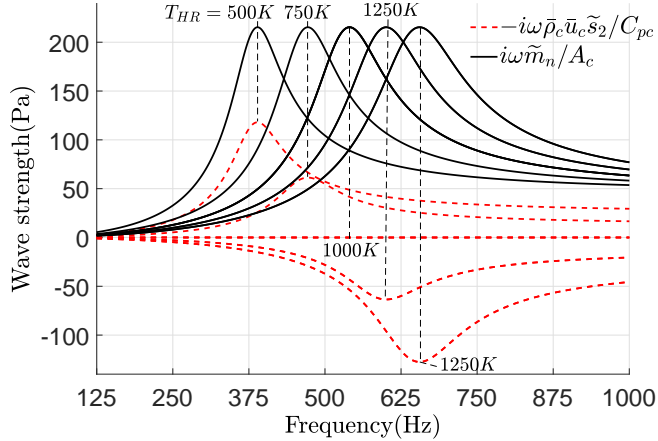


Figure 10: Case III given $\tilde{p}_1^+ = \tilde{p}_1^- = 100\text{Pa}$, $\theta = 0$. The source strengths for increasing the temperature of the HR bias flow from 500K up to 1500K, while the grazing flow temperature remains constant at 1000K

bias flow temperature from 500K to 1500K and the grazing flow temperature is maintained at 1000K. It can be seen in Fig. 9a that, when the combustor temperature is fixed at 1000K and the HR temperature is increased from 500K to 1500K, \tilde{p}_2^- is enhanced while \tilde{p}_2^+ is reduced, and the HR's sound absorption performance is progressively improved, as shown in Fig. 9c. The SEC model could not predict the correct trends, while the present model captures them, being consistent with predicting from the previous JC model. It shows that although the 500K curve and the 1500K curve have the same temperature difference between the combustor and the HR, they see completely different trends. As shown in Fig. 10 when the temperature of bias flow \bar{T}_{HR} is lower than that of the grazing flow \bar{T}_c , the entropic source have the opposite effect of the mass-related source; when $\bar{T}_c > \bar{T}_{HR}$, the entropic source has the same effect as the mass-related source—this follows the relation in Eq. (28). Furthermore, the strength of the entropy perturbation at 1500K is noticeably lower than that at 500K (see Fig. 9b), however, the strength of the entropic source has almost the same peak at both temperatures (see Fig. 10). Finally, as expected, the 1500K HR gives a higher peak sound absorption coefficient than the 1000K case, as shown in Fig. 9c.

V. Conclusion

An acoustic analogy model based on the linearised mass,momentum and energy conservation equations for a 1-D combustor duct with a Helmholtz resonator at a different temperature is derived. This provides mathematical expressions and physical insights to the sound sources of the HR in the combustor duct acoustics. The proposed acoustic analogy model was solved analytically in the frequency domain to perform a quantitative study of the acoustics of the combustor duct. A simplified acoustic analogy model is proposed and

compared to the previous Jump condition which does not provide physical mechanisms and the stagnation enthalpy continuity model which can't capture the effect of the temperature difference. The comparisons showed that the present models capture the correct entropy wave generation and changes of the acoustic fields inside the combustor. It was also confirmed that the acoustic effect of the HR depends not only on the unsteady mass injection of bias flow but also the generation of entropy perturbation after the HR due to the unsteady mixing of the bias and grazing flows (entropic source).

The entropic source term is negative compared to the mass-related source term when that of the bias flow is lower than the temperature of the grazing flow and is positive when it's higher. When the HR temperature is higher, the positive entropic source improves the HR's sound absorption performance. The simplified model shows that the overall acoustic source is a volumetric source that depends on the mean speed of sound and density of the HR instead of the combustor. Thus, when the circumstance permits, we can increase the temperature of the bias flow to improve the HR's sound absorption performance. This may provide some valuable guidance in designing Helmholtz dampers or similar structures in some practical applications.

This work makes two contributions. Firstly, we derive the first mathematical expressions for the entropic and volumetric sound source terms of the HR attached to a combustor duct with a different temperature. Secondly, based on the present model, we provide new physical insights on how the entropy wave generation affects the acoustic field, thus change the sound absorption performance of HR.

VI. Appendix

VI.A. Grazing flow Mach number

The entropy wave strength in the Jump condition model proposed by Yang and Morgans [16] is given in the form as follow

$$\tilde{S}_2 = \frac{\bar{c}_2}{\bar{M}_2} \left[\frac{\bar{c}_n^2(\gamma_2 - 1)}{\bar{c}_2^2(\gamma_n - 1)} - 1 + (\gamma_2 - 1) \left(\frac{3\bar{u}_n^2}{2\bar{c}_2^2} - \frac{\bar{M}_2^2}{2} - \frac{\bar{u}_n A_n}{i\omega V} \cdot \frac{\bar{c}_n^2}{\bar{c}_2^2} \right) \right] \cdot \frac{\tilde{m}_n}{A_c}. \quad (31)$$

During the derivation of the model for the entropy perturbation in section II.B, if we take all high-order terms into consideration, it can be expressed in a similar form as the JC model.

$$\begin{aligned} \tilde{S}_2 = & \frac{\bar{c}_2}{\bar{M}_2} \left[\frac{\bar{c}_n^2(\gamma_2 - 1)}{\bar{c}_2^2(\gamma_n - 1)} - 1 + (\gamma_2 - 1) \left(\frac{3\bar{u}_n^2}{2\bar{c}_2^2} - \frac{\bar{M}_2^2}{2} - \frac{\bar{u}_n A_n}{i\omega V} \cdot \frac{\bar{c}_n^2}{\bar{c}_2^2} \right) \right] \cdot \frac{\tilde{m}_n}{A_c} \\ & + (\gamma_2 - 1)\bar{M}_2 \left[(\tilde{p}_1^+ - \tilde{p}_1^-) - (\tilde{p}_2^+ - \tilde{p}_2^-) \right] + (\gamma_2 - 1)(\tilde{p}_1 - \tilde{p}_2). \end{aligned} \quad (32)$$

Then, by substituting Eq. (31) into Eqs. (20), we can obtain the Original Acoustic Analogy model (OAA). This takes all high-order terms into consideration. It can be expressed in form of the JC model,

$$(1 - \bar{M}_2^2) \frac{\partial \tilde{p}}{\partial x} \Big|_1 = i\omega \left[\frac{\bar{c}_n^2(\gamma_2 - 1)}{\bar{c}_2^2(\gamma_n - 1)} + (\gamma_2 - 1) \left(\frac{3\bar{u}_n^2}{2\bar{c}_2^2} - \frac{\bar{M}_2^2}{2} - \frac{\bar{u}_n A_n}{i\omega V} \cdot \frac{\bar{c}_n^2}{\bar{c}_2^2} \right) \right] \cdot \frac{\tilde{m}_n}{A_c} \\ + i\omega \left[(\gamma_2 - 1) \frac{\bar{M}_2^2}{\bar{c}_2} \left[(\tilde{p}_1^+ - \tilde{p}_1^-) - (\tilde{p}_2^+ - \tilde{p}_2^-) \right] + (\gamma_2 - 1) \frac{\bar{M}_2}{\bar{c}_2} (\tilde{p}_1 - \tilde{p}_2) \right], \quad (33)$$

$$(1 - \bar{M}_2^2) \tilde{p}|_1^2 = \left[\frac{\bar{c}_n^2(\gamma_2 - 1)}{\bar{c}_2^2(\gamma_n - 1)} + 1 + (\gamma_2 - 1) \left(\frac{3\bar{u}_n^2}{2\bar{c}_2^2} - \frac{\bar{M}_2^2}{2} - \frac{\bar{u}_n A_n}{i\omega V} \cdot \frac{\bar{c}_n^2}{\bar{c}_2^2} \right) \right] \cdot \bar{u}_2 \frac{\tilde{m}_n}{A_c} \\ + \left[(\gamma_2 - 1) \bar{M}_2^3 \left[(\tilde{p}_1^+ - \tilde{p}_1^-) - (\tilde{p}_2^+ - \tilde{p}_2^-) \right] + (\gamma_2 - 1) \bar{M}_2^2 (\tilde{p}_1 - \tilde{p}_2) \right]. \quad (34)$$

The above derivations consider only low-Mach-number $\bar{M}_1 \ll 1$, in which case keeping only the terms of order $O(M)$ is sufficient. When this is not satisfied, at least the term of order $O(M^2)$ should be retained in the process of derivation. In this case, all the terms should be retained in Eq. (16). Hence, a model for entropy perturbation is given by Eq. (32) in this Appendix, which is in the same form shown in the work of Yang and Morgans [16]. For convenience, the results obtained by solving Eqs. (32) and (20) is called the Original Acoustic Analogy model (OAA) for it takes all high-order terms into consideration. The influence of the grazing flow Mach number on the accuracy of the present model is studied by comparing predictions which retaining only the $O(M)$ term (SAA/AA), and those retaining all high-order terms $O(M^2)$ (OAA) for various (low) grazing flow Mach numbers. This is shown in Figure 11.

Figure. 11 shows that the peaks of \tilde{p}_2^- and the minimum values of \tilde{p}_2^+ respectively increase and decrease with the grazing flow Mach number for all models, indicating that an asymmetry is introduced by the grazing flow. This asymmetry increases with the increase of the Mach number. Predictions from the JC model and the OAA model agree very well at all given Mach numbers. However, predictions from the AA model no longer give sufficient accuracy at $\bar{M}_1 = 0.3$ but provides satisfactory accuracy at $\bar{M}_1 = 0.165$. The results from SAA ensure sufficient accuracy only at $\bar{M}_1 = 0.03$.

To summarize, in sufficiently low Mach number conditions, the SAA is sufficient for required accuracy. The OAA model provides the best accuracy when the low-Mach number condition is not strictly satisfied.

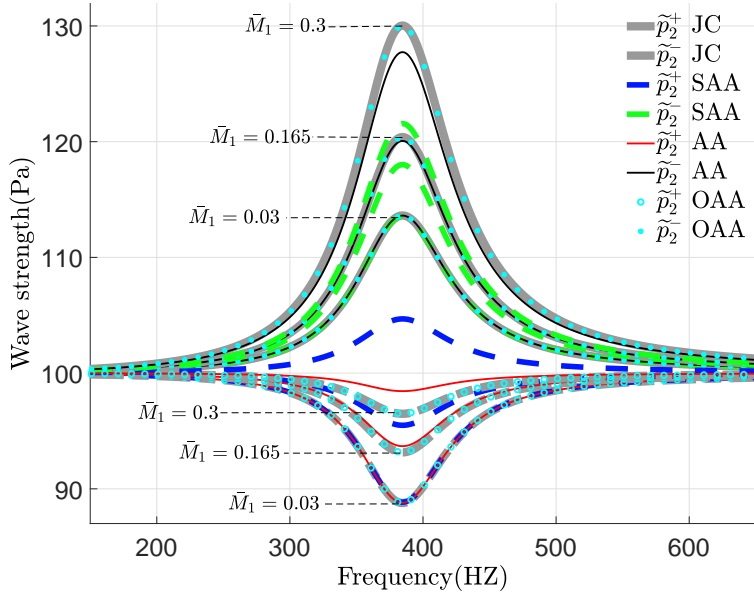


Figure 11: Case III given $\tilde{p}_1^+ = \tilde{p}_1^- = 100\text{Pa}$, $\theta = 0$. The acoustic wave strengths of different models comparing the effects of various grazing flow Mach number with $\bar{T}_c = 1000\text{K}$ and $\bar{T}_{HR} = 500\text{K}$.

VII. Acknowledgments

This work has been supported by the National Natural Science Foundation of China (grant No.52106159) which is gratefully acknowledged by the authors.

References

- [1] S. M. Correa. “Power generation and aeropropulsion gas turbines: From combustion science to combustion technology”. In: *Symposium (International) on Combustion*. Vol. 27. 2. Elsevier. 1998, pp. 1793–1807. DOI: [https://doi.org/10.1016/S0082-0784\(98\)80021-0](https://doi.org/10.1016/S0082-0784(98)80021-0).
- [2] T. Lieuwen. “Modeling premixed combustion-acoustic wave interactions: A review”. In: *Journal of Propulsion and Power* 19.5 (2003), pp. 765–781. DOI: [10.2514/2.6193](https://doi.org/10.2514/2.6193).
- [3] A. P. Dowling and S. R. Stow. “Acoustic analysis of gas turbine combustors”. In: *Journal of Propulsion and Power* 19.5 (2003), pp. 751–764. DOI: [10.2514/2.6192](https://doi.org/10.2514/2.6192).
- [4] T. Poinsot. “Prediction and control of combustion instabilities in real engines”. In: *Proceedings of the Combustion Institute* (2016). DOI: [10.1016/j.proci.2016.05.007](https://doi.org/10.1016/j.proci.2016.05.007).
- [5] S. Candel. “Combustion dynamics and control: Progress and challenges”. In: *Proceedings of the Combustion Institute* 29.1 (2002). Proceedings of the Combustion Institute, pp. 1–28. ISSN: 1540-7489. DOI: [https://doi.org/10.1016/S1540-7489\(02\)00001-1](https://doi.org/10.1016/S1540-7489(02)00001-1)

7489(02)80007–4. URL: <https://www.sciencedirect.com/science/article/pii/S1540748902800074>.

- [6] T. C. Lieuwen and V. Yang. *Combustion instabilities in gas turbine engines: operational experience, fundamental mechanisms, and modeling*. American Institute of Aeronautics and Astronautics, 2005. doi: <https://doi.org/10.2514/4.866807>.
- [7] I. Hughes and A. Dowling. “The absorption of sound by perforated linings”. In: *Journal of Fluid Mechanics* 218 (1990), pp. 299–335. doi: <https://doi.org/10.1017/S002211209000101X>.
- [8] J. D. Eldredge and A. P. Dowling. “The absorption of axial acoustic waves by a perforated liner with bias flow”. In: *Journal of Fluid Mechanics* 485 (2003), pp. 307–335. doi: [10.1017/S0022112003004518](https://doi.org/10.1017/S0022112003004518).
- [9] V. Bellucci, P. Flohr, C. O. Paschereit, and F. Magni. “On the use of Helmholtz resonators for damping acoustic pulsations in industrial gas turbines”. In: *Journal of Engineering for Gas Turbines and Power* 126.2 (2004), pp. 271–275. doi: [10.1115/2001-GT-0039](https://doi.org/10.1115/2001-GT-0039).
- [10] D. Zhao and X. Li. “A review of acoustic dampers applied to combustion chambers in aerospace industry”. In: *Progress in Aerospace Sciences* 74 (2015), pp. 114–130.
- [11] M. Howe. “Attenuation of sound in a low Mach number nozzle flow”. In: *Journal of Fluid Mechanics* 91.2 (1979), pp. 209–229.
- [12] D. Bechert. “Sound absorption caused by vorticity shedding, demonstrated with a jet flow”. In: *Journal of Sound and Vibration* 70.3 (1980), pp. 389–405.
- [13] A. Cummings. “Acoustic nonlinearities and power losses at orifices”. In: *AIAA Journal* 22.6 (1984), pp. 786–792. doi: [10.2514/3.8680](https://doi.org/10.2514/3.8680).
- [14] I. D. J. Dupère and A. P. Dowling. “The use of Helmholtz resonators in a practical combustor”. In: *Journal of Engineering for Gas Turbines and Power* 127.2 (2005), pp. 268–275. doi: [10.1115/1.1806838](https://doi.org/10.1115/1.1806838).
- [15] D. Zhao, C. A’Barrow, A. S. Morgans, and J. F. Carrotte. “Acoustic damping of a Helmholtz resonator with an oscillating volume”. In: *AIAA Journal* 47.7 (2009), pp. 1672–1679. doi: [10.2514/1.39704](https://doi.org/10.2514/1.39704).
- [16] D. Yang and A. S. Morgans. “Acoustic models for cooled helmholtz resonators”. In: *AIAA Journal* 55.9 (2017), pp. 3120–3127. doi: <https://doi.org/10.2514/1.J055854>.

- [17] W. K. Blake, S. Candel, D. Crigthon, F. Farassat, J. F. Williams, A. George, M. Howe, A. Nayfeh, A. Powell, N. Rott, et al. “Recent Advances in Aeroacoustics: Proceedings of an International Symposium Held at Stanford University, August 22–26, 1983”. In: (2012).
- [18] Z. Gan and D. Yang. “An acoustic analogy model for Helmholtz resonators with cooling bias flow”. In: *Chinese Journal of Theoretical and Applied Mechanics* 54.3 (2022), pp. 1–11. DOI: [10.6052/0459-1879-21-561](https://doi.org/10.6052/0459-1879-21-561).
- [19] J. Li and A. S. Morgans. “Simplified models for the thermodynamic properties along a combustor and their effect on thermoacoustic instability prediction”. In: *Fuel* 184 (2016), pp. 735–748. DOI: [10.1016/j.fuel.2016.07.050](https://doi.org/10.1016/j.fuel.2016.07.050).
- [20] J. J. Keller and E. Zauner. “On the use of Helmholtz resonators as sound attenuators”. In: *Zeitschrift für angewandte Mathematik und Physik ZAMP* 46.3 (1995), pp. 297–327. DOI: <https://doi.org/10.1007/BF01003552>.
- [21] B. Ćosić, T. G. Reichel, and C. O. Paschereit. “Acoustic Response of a Helmholtz Resonator Exposed to Hot-Gas Penetration and High Amplitude Oscillations”. In: *Journal of Engineering for Gas Turbines and Power* 134.10 (2012), p. 101503. DOI: [10.1115/1.4007024](https://doi.org/10.1115/1.4007024).
- [22] B. Ćosić, D. Wassmer, S. Terhaar, and C. O. Paschereit. “Acoustic response of Helmholtz dampers in the presence of hot grazing flow”. In: *Journal of Sound and Vibration* 335 (2015), pp. 1–18. DOI: [10.1016/j.jsv.2014.08.025](https://doi.org/10.1016/j.jsv.2014.08.025).
- [23] M. Betz, M. Zahn, C. Hirsch, and T. Sattelmayer. “Impact of Combustion Chamber Dynamics on the Temperature Distribution in a Resonator”. In: *Turbo Expo: Power for Land, Sea, and Air*. Vol. 58615. American Society of Mechanical Engineers. 2019, V04AT04A012. DOI: [10.1115/GT2019-90239](https://doi.org/10.1115/GT2019-90239). URL: <https://doi.org/10.1115/GT2019-90239>.
- [24] M. S. Howe. “On the theory of unsteady high Reynolds number flow through a circular aperture”. In: *Proceedings of the Royal Society of London. A. Mathematical and Physical Sciences* 366.1725 (1979), pp. 205–223. DOI: [10.1098/rspa.1979.0048](https://doi.org/10.1098/rspa.1979.0048).
- [25] J. Rupp, J. Carrotte, and A. Spencer. “Interaction between the acoustic pressure fluctuations and the unsteady flow field through circular holes”. In: *Journal of Engineering for Gas Turbines and Power* 132.6 (2010). URL: <https://doi.org/10.1115/1.4000114>.
- [26] C. L. Morfey. “Sound transmission and generation in ducts with flow”. In: *Journal of Sound and Vibration* 14.1 (1971), pp. 37–55. DOI: [10.1016/0022-460X\(71\)90506-2](https://doi.org/10.1016/0022-460X(71)90506-2).